Profiling multi-body interactions of BCL2 with single-molecule co-immunoprecipitation reveals the molecular mechanism of ABT-199 resistance

Authors

Changju Chun[1] and Tae-Young Yoon[1*]

Affiliations

1. School of Biological Sciences and Institute for Molecular Biology and Genetics, Seoul National University, Seoul 08826, South Korea

* Corresponding author. Email: tyyoon@snu.ac.kr

Abstract

A capability to characterize protein-protein interactions (PPIs) in a quantitative manner with an increased speed would form a technical basis for accelerating drug discovery targeting the PPI network. We here used the single-molecule pull-down and co-IP platform to examine PPI between BCL2 and BH3-only proteins in crude extract environments. We focused on how the PPI strengths changed with single-point BCL2 mutations found in relapsed chronic lymphocytic leukemia showing ABT-199 resistance, where we took a mix-and-match approach to examine various pairs of baits and preys while titrating their concentrations. This allowed us to examine total 21 PPI reactions and 420 data points, forming a high-resolution large data set of the dissociation constants (K_d) and the drug inhibitory constants (K_i). Our data suggest that the different BCL2 mutants take different routes to acquire resistance to ABT-199, demonstrating how large-scale, quantitative PPI data sets reveal insights into the evolving dynamics of PPI networks.

Introduction

Protein-protein interactions (PPIs) form the intricate web through which cellular information is transmitted.[1-3] Selectively amplifying or diminishing specific PPI subsets can alter these networks' equilibrium, thereby adjusting the flow of signals across various pathways and enabling cells to navigate ever-changing environments. The fine-tuning of PPI intensities is facilitated by various biochemical mechanisms, such as post-translational modifications, scaffolding proteins, and the condensation of intrinsically disordered regions.[4-6] A quantitative assessment of the strengths of these protein-protein connections, many involving complex multi-body interactions, would enhance our comprehension of PPI networks and their adaptive evolution.

Currently, surface plasmon resonance (SPR) is the benchmark for quantifying PPIs, offering label-free interaction monitoring.[7] However, SPR signals can be challenging to decipher, especially with multi-body interactions, because the absence of labels complicates the identification of signal origins.[8] Additionally, SPR typically demands large sample volumes due to measurements at various concentration levels and the necessity of continuous sample flow, resulting in lengthy assessment times for each PPI pair.[8-9] Therefore, there is a significant opportunity for advancements in high-throughput techniques capable of characterizing multi-body interactions involving multiple protein and small molecule pairs.

Apoptosis is an evolutionarily conserved form of programmed cell death that is important for removing abnormal cells such as cancer cells while causing minimal damage to surrounding tissues.[10-11] The BCL2 protein family regulates initiation of the apoptosis, and the delicate balance between the various PPIs among its members determines cell fate.[12] The primary effectors of apoptosis, BAX and BAK, form pores on mitochondrial outer membranes upon undergoing conformational changes triggered by the binding of BH3-only proteins, such as BIM, BAD, and BID.[13-17] Another group of BCL2 proteins, which includes BCL2 itself, as well as BCLxL and MCL1, interacts with both these effectors and the BH3-only proteins.[12, 18-19] In many cancers, PPIs involving anti-apoptotic proteins are found to be upregulated than is found in normal cells,[19-23] effectively preventing interactions between the effectors and the pro-apoptotic BH3-only proteins and thereby preventing apoptosis initiation.[24-26]

Therapeutic agents, referred to as BH3 mimetics, structurally emulate the alpha-helical

31   BH3 domain and are designed to bind anti-apoptotic proteins. This binding effectively releases

32   and/or prevents any further binding with pro-apoptotic proteins,[27-28] making BH3 mimetics a

33   salient example of a PPI inhibitor.[29-31] Indeed, ABT-199, which specifically inhibits the PPIs of

34   BCL2 and not BCLxL or MCL1,[30] was approved for the treatment of chronic lymphocytic

35   leukemia (CLL) in 2016 (NCT01889186), and acute myeloid leukemia (AML) in 2018

36   (NCT02203773 and NCT02287233). Despite a remarkable initial response rate in phase I trials

37   for relapsed/refractory CLL or small lymphocytic leukemia (SLL), 27% of patients showed

38   regression within 15 months of ABT-199 treatment,[32-33] often associated with BCL2 mutations

39   such as G101V.[34-35] The aspartate residue at position 103, which lines the binding groove of

40   BCL2, was also found to be a hotspot, with various single residue substitutes, including tyrosine

41   (D103Y), glutamine (D103E), and valine (D103V) found in relapsed CLL patients.[36-37] This

42   illustrates how single point mutations in BCL2 can disrupt PPIs between various BH3-only

43   proteins and effectors to affect the balance of the whole PPI network. It also provides an example

44   that underscores the need for quantitative characterization of PPI networks on a larger scale.

45   Single-molecule pull-down and co-IP (SMPC) is a platform that can assess PPI strength

46   under crude lysate conditions.[38-39] In this platform, bait proteins are immobilized on a surface via

47   antibody binding. Then, prey proteins labeled with enhanced green fluorescent proteins (eGFPs)

48   are added and allowed to freely diffuse and interact with bait. The formation of a single PPI

49   complex between bait and prey can then be detected as a stable diffraction-limited fluorescence

50   spot under a total internal reflection (TIR) fluorescence microscope with single-molecule

51   resolution.[38-39] Counting these single PPI complexes within a fixed area provides a rapid way to

52   quantify PPI strength. SMPC has been used to examine the PPI networks of various isoforms of

53   RAS proteins,[40] epidermal growth factor receptors,[41] as well as their heterodimer complexes,[42]

54   all of which work as oncoproteins (or onco-complexes) driving the progression of different types

55   of cancers. In particular, the PPI strengths determined by SMPC have proven to have highly

56   quantitative correlations with the effectiveness of targeted drugs.[41]

57   Here, we employed the SMPC platform for a quantitative examination of PPIs between

58   BCL2 and BH3-only proteins. Taking advantage of the robustness and speed of the SMPC

59   platform, we generated a large-scale data set encompassing 420 different PPI reactions, including

60   those between BCL2 containing single-point mutations found in relapsed CLL patients and

61 various splice variants of BH3-only proteins. By titrating prey and drug concentrations, we were

62 able to determine dissociation constants (K_d) of PPI and drug inhibitory constants (K_i) for ABT-

63 199. With the increased throughput and quantitativeness provided by this technique, we were

64 able to identify the changes in the K_d and K_i values for each interaction with the various BCL2

65 mutants. Our results point to the different routes by which BCL2 mutations can lead to ABT-199

66 resistance.

67

Results and Discussion

Application of SMPC to the BCL2 PPI network

70 To investigate the PPI network with a focus on the anti-apoptotic BCL2 protein, we employed

71 the SMPC platform. We engineered a fusion of a red fluorescent protein (RFP, specifically

72 mCherry) to the C-terminus of the *BCL2* gene, promoting transient expression of BCL2-mCherry

73 in HEK293T cells (Figure 1A). Given that BCL2 proteins possess a single transmembrane

74 domain (TMD),[43] we extracted the fluorescently labeled BCL2 using mild cholesterol-mimicking

75 detergents, as our prior work validated this method for preserving surrounding membrane

76 patches.[42] Anti-RFP antibodies, layered atop polyethylene glycol (PEG) polymers, allowed us to

77 immobilize BCL2 proteins directly from cell extracts onto a surface while minimizing the

78 nonspecific binding of other proteins (Figure 1A and Figure S1). This strategy leverages the

79 absence of mCherry homologs in mammalian proteomes to reduce the risk of nonspecific

80 immunoprecipitation. In separate cultures, we expressed various BH3-only proteins tagged with

81 eGFPs (Figure 1B). Lysis of these cells followed by dilution produced extracts with a consistent

82 concentration (typically 10 nM) of the targeted BH3-only protein. These extracts were then

83 introduced into the reaction chamber to initiate PPIs (Figure 1B).

84 Single-molecule fluorescence imaging, averaged over hundreds of milliseconds,

85 effectively eliminated the signal from unbound eGFP-tagged proteins due to rapid diffusion,

86 resulting in a diffuse background. In contrast, eGFP-labeled proteins bound to immobilized

87 BCL2 molecules produced sharp, diffraction-limited spots (Figure 1B, inset). We quantified

88 these discrete PPI complexes across approximately 12 fields of view (50×100 µm²) to bolster the

89 statistical reliability of our data. This quantification process, facilitated by an automated focusing

90   system and a robotic stage on our SMPC setup, is completed within a minute (Figure S1).
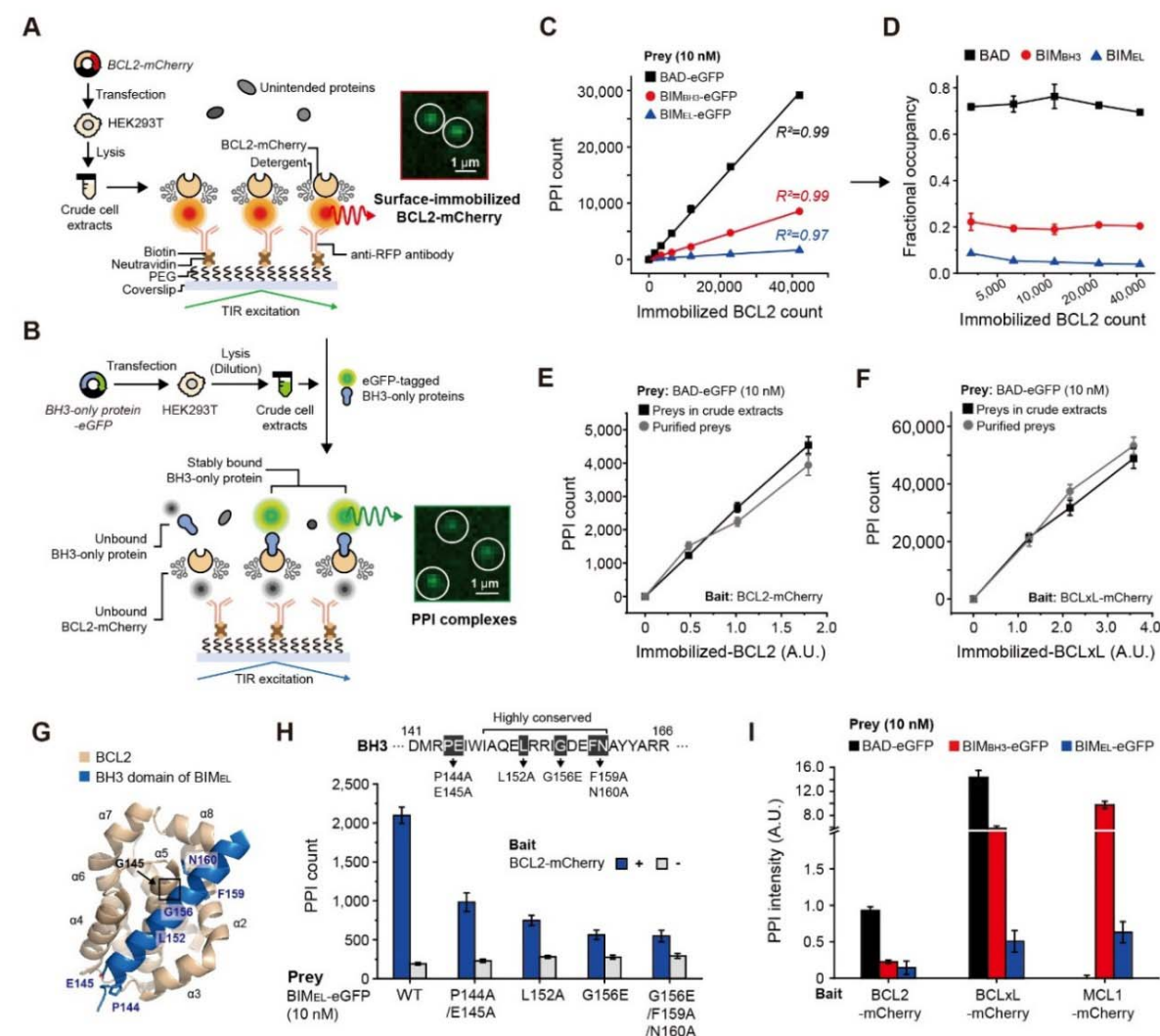

91

Figure 1. Application of SMPC platform to measure PPIs of BCL2 family members. (A) Schematic for the surface immobilization of mCherry-labeled bait proteins (BCL2-mCherry) overexpressed in HEK293T cells. Bait proteins were selectively immunoprecipitated with a biotinylated anti-RFP antibody. Immobilized bait proteins were observed as defined spots of fluorescent signal (inset). (B) PPIs were initiated by adding eGFP-labeled BH3-only proteins (BAD, BIM_{BH3}, and BIM_{EL}) overexpressed in HEK293T cells. Prey proteins selectively interacted with immobilized bait proteins. PPI complexes appeared as distinct spots of fluorescent signal (inset). (C) Linear increase in the PPI count with increasing amounts of surface-immobilized BCL2 in the presence of 10 nM of eGFP-labeled BH3-only proteins. (D) Remaining of fractional occupancies with increasing amounts of surface-immobilized BCL2. (E and F) Comparison of the PPIs by the BAD preys in crude extracts and the purified BAD preys. (E) BCL2-BAD PPIs, (F) BCLxL-BAD PPIs. (G) Structure of the $BCL2-BIM_{BH3}$ complex as predicted by AlphaFold2. Highly conserved residues on the BH3 domain of BIM are labeled. G156 on the BH3 domain is located adjacent to G145 on BCL2 (inset). (H) Changes in the PPI count between BCL2 and BH3 domain mutated BIM_{EL}. (I) PPIs for various pairs of mCherry-labeled anti-apoptotic proteins (BCL2, BCLxL, and MCL1) and eGFP-labeled BH3-only proteins (BAD, BIM_{BH3}, and BIM_{EL}).

106   Upon introducing different pro-apoptotic BH3-only proteins as preys at a concentration

107 of 10 nM, the number of PPIs rose linearly with the increasing number of immobilized BCL2

108 proteins per field of view (up to 40,000) (Figure 1C). These findings demonstrated that the BCL2

109 proteins' fractional occupancy remained essentially unchanged, even with an ~20-fold increase in

110 BCL2 pull-down numbers (Figure 1D). This constancy implies that the prey proteins in the

111 reaction chambers were not depleted and could sustain equilibrium reactions, even at the highest

112 surface densities tested (approximately 8 baits per μm², as shown in Figure 1D). Consequently,

113 the occupancy values ascertained through SMPC could be directly applied to calculate the

114 dissociation constant (K_d) values for individual binding reactions (see below).

115 Subsequently, we aimed to discern the impact of endogenous proteins in the extracts on

116 reconstituted target PPI reactions. Employing the protocol described above, we overexpressed

117 BAD proteins in HEK293T cells and diluted the resultant extract to achieve a target BAD protein

118 concentration of 10 nM (Figure S2A). Repeated trials produced diluted extracts with total protein

119 concentrations (C_{tot}) near 0.1 mg/ml, a dilution exceeding 1,000-fold from native cellular

120 conditions. Adding BAD-eGFP proteins in crude extracts as preys, we found the BCL2 and

121 BCLxL surface baits' occupancy remained consistent, mirroring results from Figure 1D (Figure

122 1E, F, black). Remarkably, when comparing PPI reactions utilizing preys in crude extracts with

123 those incorporating purified preys at 10 nM, the binding numbers and occupancy rates for the

124 BCL2 and BCLxL baits were identical (Figure 1E, F, and Figure S3).

125 These results imply that overexpression, when effectively achieved, renders endogenous

126 proteins negligible in their effect on reconstituted target PPI reactions. We further supplemented

127 the prey protein solution with dense HEK293T cell extracts, investigating alterations in binding

128 counts within more concentrated extract conditions (Figure S2A). Intriguingly, 90% of the

129 binding was retained even with C_{tot} in the extract raised to 0.4 mg/ml in extract conditions

130 (Figure S2B, C). We then varied the total protein concentration of the extract for weaker PPI

131 reactions between BCL2 and BIM variants, which are characterized by K_ds in the tens of nM

132 range (see Figure 2 below). Despite the anticipated increased competition from endogenous

133 proteins due to the weaker interaction, the binding count consistently remained at 90% up to C_{tot}

134 of 0.4 mg/ml (Figure S2D-F). Accordingly, our proposed method for analyzing PPIs using the

135 SMPC platform has proven to generate reliable PPI counts, even amidst the challenges of a dense

136 extract milieu.

137   Next, to assess the specificity of the reconstituted target PPI reactions within the SMPC

138   platform, we introduced mutations into conserved residues within the BH3 domain of BIM_{EL}, the

139   longest splice variant of BIM [44-45]. Analysis revealed a progressive decline in PPI counts with

140   increased evolutionary conservation of the residue, as evidenced by a marked decrease in

141   interactions upon mutation of the highly conserved G156 residue (Figure 1G, H).[15, 17, 46-47] This

142   interaction was barely discernible from that of a negative control reaction (Figure 1H). This data

143   underscores the pivotal role of the conserved BH3 domain in mediating the reconstituted PPIs

144   between BCL2 and BH3-only proteins.

145   Significantly, the basic technical requirements for the SMPC assay—the overexpression

146   of target proteins in mammalian cells—facilitates a versatile combination of baits and preys

147   (Figure S4). This enabled the exploration of PPIs across a range of protein pairs extending

148   beyond the BCL2 bait. We diversified our study by surface-immobilizing BCLxL- or MCL1-

149   mCherry bait proteins as alternatives to BCL2, introducing a variety of BH3-only prey proteins.

150   This strategic approach yielded PPI counts for an array of bait-prey configurations and revealed

151   significant aspects of the BCL2 family's PPI network, including the remarkably high-affinity

152   interaction between BAD and BCLxL, which was conspicuously absent in the reactions

153   involving MCL1 (Figure 1I).[12, 19]

154

Profiling PPIs between BCL2 and splice variants of BIM

156   We utilized our SMPC platform to quantitatively ascertain the K_d values for multiple protein-

157   protein interactions. To test the platform's ability to distinguish between PPIs of closely related

158   but distinct proteins, we evaluated several BIM splice variants (BIM_{EL}, BIM_L, BIM_S, and

159   BIM_{XS}), which differ in their N-terminal exon domains preceding the BH3 domain (Figure

160   2A).[44-45] According to the established structures of the BCL2-BIM complex, the BCL2 binding

161   groove accommodates only the BH3 domain.[28] AlphaFold2 predictions failed to provide a

162   defined structure for these N-terminal domains of BIM alone or in complex with BCL2,[48-49]

163   hinting that areas other than the BH3 domain may be disordered even when BCL2 is present

164   (Figure 2B, C, and Figure S5). Therefore, our comparison across the BIM variants aimed to

165   understand the influence of these intrinsically disordered regions on PPI stability.
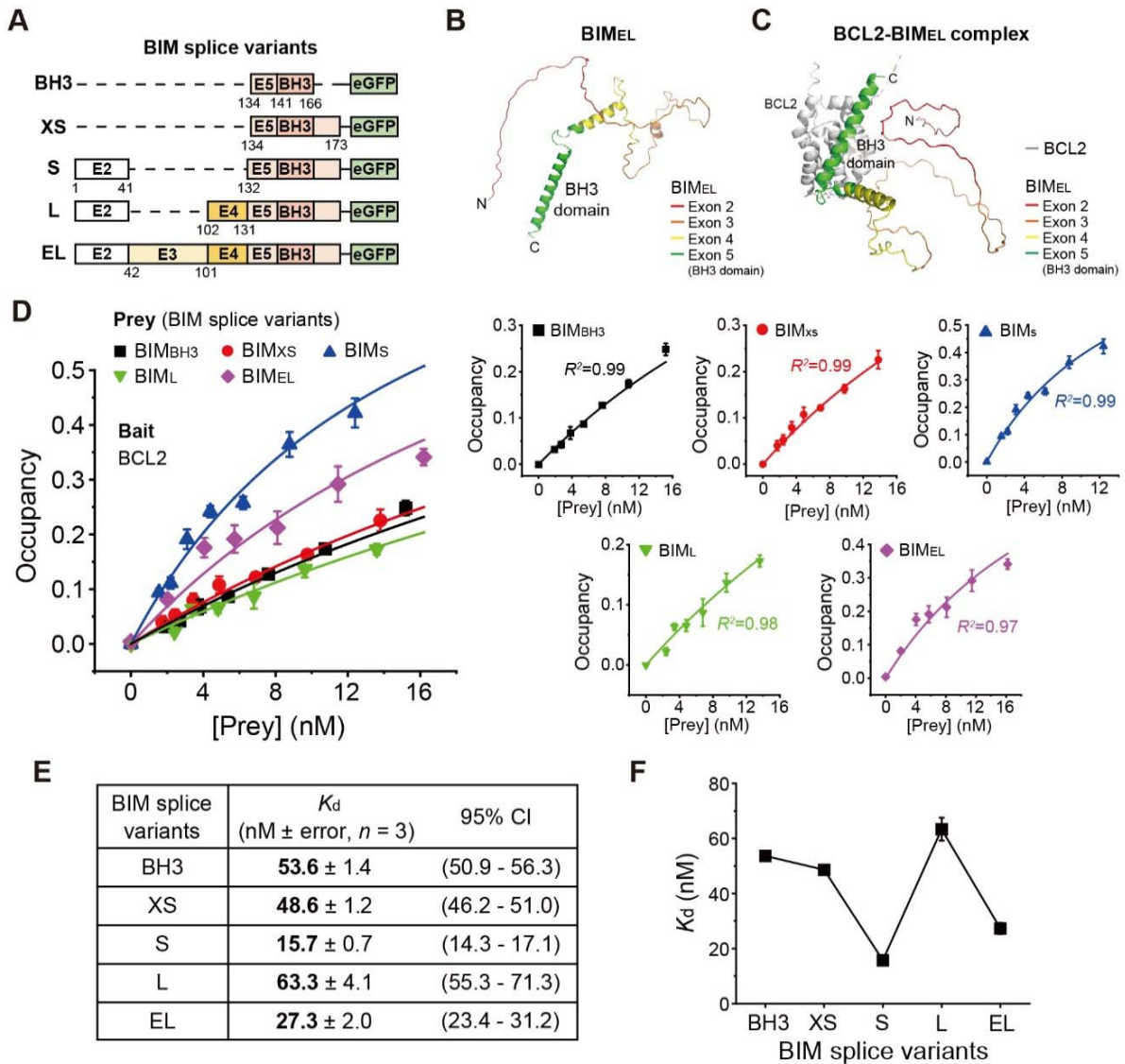
7

166

Figure 2. N-terminal exon domains of BIM make distinct contributions to BCL2 PPIs. (**A**) TMD-truncated BIM splice variant (BIM_{BH3}, BIM_{XS}, BIM_S, BIM_L, and BIM_{EL}) constructs. E2-E5 refer to each exon domain. (**B**) Predicted structure of BIM_{EL} by AlphaFold2. TMD sequence of BIM was removed for structure prediction. (**C**) Predicted structure of BCL2-BIM_{EL} by AlphaFold2. TMD sequences of BCL2 and BIM were removed, and the $(GGSG)_4$ linker was inserted between the C-terminus of BCL2 and the N-terminus of BIM_{EL} for structure prediction. (**D**) Binding curves for each BIM splice variant to BCL2 used for K_d fitting. All data were fitted with equation (1) in the Methods section. The binding curves accoring to prey proteins are individually displayed. Data are presented as means $\pm$ s.d. ($n = 3$). (**E**) Fitted K_d and 95% confidence intervals (CI) for PPIs between BCL2 and BIM splice variants. (**F**) Dynamic changes in K_d according to BIM splicing.

In optimizing the experimental setup to evaluate PPI strength between BCL2 and BIM variants, when using the BIM_{EL} variant with its transmembrane domain (TMD) intact, we noted that its PPI counts were subtly influenced by the type of detergents in the reaction buffer (Figure S6A). Consequently, we chose to analyze the PPIs of the TMD-truncated BIM variants in a

8

180   buffer containing 0.03% Triton X-100, which not only increased the PPI count numbers per se

181   and but also improved the consistency of our SMPC experiments across multiple repetitions

182   (Figure S6B). We noted occasional cleavage of fluorescent tags from prey proteins (Figure S6C-

183   E) but, aside from BIM_{XS}, consistently found the remaining intact portion to exceed 60% for all

184   variants assessed. This cleaved fraction was accounted for in our K_d calculations unless

185   otherwise stated (and K_i values, see below).

186   When we immobilized a constant amount of BCL2-mCherry proteins (~2,000 per field of

187   view), we added the BH3 domain of BIM (BIM_{BH3}) in increasing concentrations to determine

188   PPI counts. These counts were converted into occupancy values, representing the ratio of BCL2-

189   mCherry proteins bound by an eGFP-tagged prey protein. By plotting these occupancy values

190   against the BIM_{BH3} concentrations, we deduced a K_d of 53.6±1.4 nM with an intra-assay

191   coefficient of variance (CV) of approximately 6.6% (Figure 2D, E, and table S1).

192   In extending our analysis to additional BIM splice variants, we encountered an intriguing

193   observation: the length of the splice variant did not correlate with a simple increase or decrease

194   in occupancy value (Figure 2D-F). Instead, we observed complex patterns in the binding curves,

195   indicative of the unique influence each exon domain has on BIM's affinity for BCL2. The

196   inclusion of the E2 domain (BIM_S) significantly raised the occupancy values, thereby reducing

197   the K_d from 53.6 nM to 15.7 nM (Figure 2D-F). Conversely, incorporating the E4 domain (BIM_L

198   as opposed to BIM_S) resulted in a marked decrease in occupancy, increasing the K_d to 63.3 nM

199   (Figure 2D-F). These findings demonstrate that while the E2 domain promotes BCL2-BIM PPIs,

200   the E4 domain undermines them. Introducing the E3 domain between E2 and E4 (BIM_{EL} versus

201   BIM_L) increased the binding curve, yielding a K_d of 27.3 nM, signifying that the presence of E3

202   considerably strengthens the BCL2-BIM interaction (Figure 2D-F).

203   Together, the SMPC platform enables swift PPI count determination for 40 different

204   reactions, while demanding minimal experimental requirements. The resulting data sets reveal

205   the individual contributions of domains to the BCL2-BIM interaction. Our data suggest that the

206   BIM isoforms have varying and dynamic influences on apoptotic regulation through their

207   differential affinities for BCL2 and other anti-apoptotic proteins.

208

209 **Profiling multi-body interactions between BCL2 family proteins and ABT-199**

210 We subsequently leveraged our platform to investigate the impact of BCL2 mutations, G101V

211 and D103E, identified in relapsed CLL patients post-ABT-199 therapy, on the complex interplay

212 among BCL2, BH3-only proteins, and ABT-199. These mutations reside within the second alpha

213 helix of BCL2, in a region critical for binding both the BH3 domain and ABT-199, suggesting

214 they could modulate the affinity of BCL2 for its BH3-only protein ligands and for ABT-199
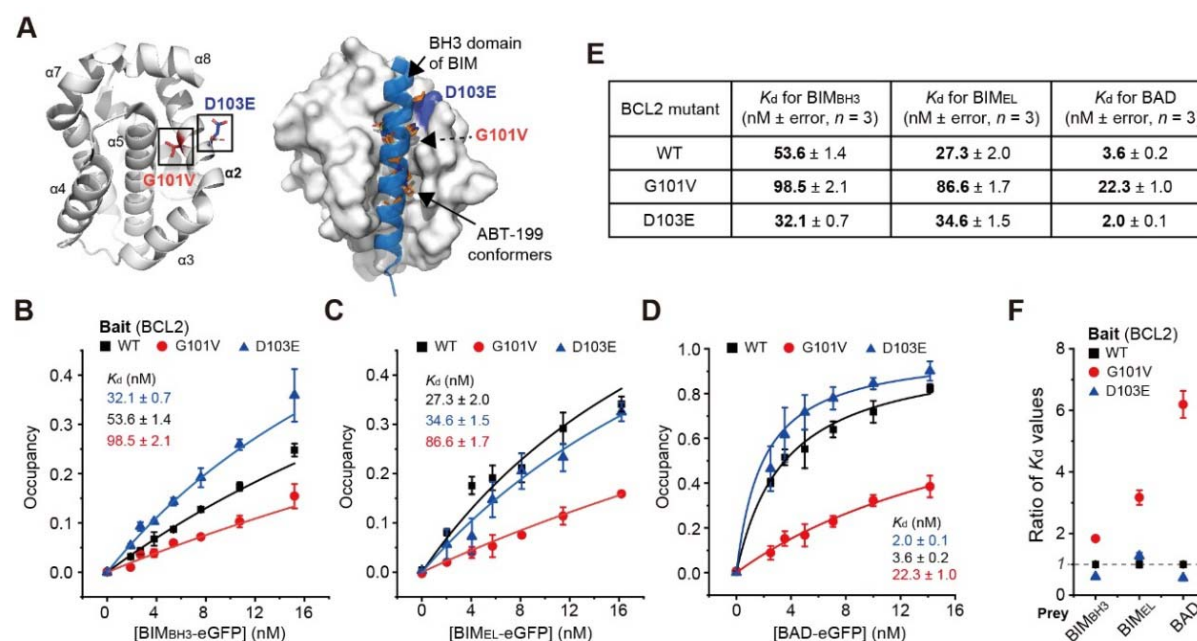
215 (Figure 3A).[35, 37]

216

217 **Figure 3. G101V and D103E mutants have opposite effects on BCL2's interactions with BH3-only proteins. (A)**
218 Predicted BCL2 structures showing mutated residues (G101V and D103E) in comparison with the PDB structure
219 (PDB id: 6O0K). BCL2 is shown in white, the BH3 domain of BIM is shown in blue, and ABT-199 conformers are
220 shown in orange. G101 (V101) and D103 (E103) residues on the BCL2 are labeled. (**B-D**), Binding curves for each
221 BH3-only protein to mutant BCL2s for K_d fitting. (B) BCL2-BIM$_{BH3}$ PPIs, (C) BCL2-BIM$_{EL}$ PPIs, and (D) BCL2-
222 BAD PPIs. All data were fitted with equation (1) in the Methods section. Data are presented as means ± s.d. ($n = 3$).
223 (**E**) Fitted K_d for PPIs between mutant BCL2s (WT, G101V, and D103E) and BH3-only proteins (BIM$_{BH3}$, BIM$_{EL}$,
224 and BAD). The 95% CI values are described in Table S2. (**F**) Comparing the ratio of K_d values relative to BCL2$_{WT}$
225 PPIs.

226 The reductionist's nature of SMPC enabled us to reconstruct these intricate interactions

227 incrementally, beginning with the BCL2 interactions with a suite of BH3-only proteins, followed

228 by the introduction of the BH3 mimetic, ABT-199, to evaluate its impact on these interactions.

229 As predicted by the steric properties of valine, and in agreement with existing literature, the

230 G101V mutation notably disrupted the interactions between BCL2 and all tested BH3-containing

10

231 proteins (BIM$_{BH3}$, BIM$_{EL}$, and BAD) (Figure 3B-F).[34-35] The D103E mutation, however,

232 conferred a modest yet significant increase in the binding affinity of BCL2 for BIM$_{BH3}$, lowering

233 the K_d from 53.6±1.4 nM (wild-type BCL2) to 32.1±0.7 nM (Figure 3B, E). These binding

234 profiles were obtained by averaging the outcomes of three distinct experiments, thereby allowing

235 us to discern relatively small shifts in K_d values (with an intra-assay coefficient of variation of

236 8.7%) (Tables S2 and S3). In assays with BIM$_{EL}$, the D103E mutation resulted in a decreased

237 affinity relative to wild-type BCL2. Hence, the presence of the D103E mutation unfavorably

238 altered the interaction between BCL2 and BIM$_{EL}$'s N-terminal disordered domains (E2 to E4),

239 negating the enhanced binding observed with BIM$_{BH3}$ and BCL2$_{D103E}$ (Figure 2A, and Figure 3C,

240 E). Employing full-length BAD as the prey molecule yielded analogous shifts in binding

241 dynamics: G101V mutation resulted in substantial inhibition, whereas D103E mutation slightly

242 but significantly strengthened the PPI (Figure 3D, E).

243 To quantify the effects of ABT-199 on the PPIs of each BCL2 mutant, we mixed ABT-

244 199 with the BH3-only prey proteins under a set of designated conditions and counted the

245 residual PPI complexes (Figure 4A). As anticipated, the more ABT-199 were included, the lower

246 the residual PPI count, indicating competition among the prey molecules and ABT-199 for BCL2

247 binding. By fitting the inhibition curves of eight different ABT-199 concentrations, all with WT

248 BCL2 as the bait, we were able to determine K_i values of 17.5 ± 1.0, 53.7 ± 4.8, and 4.4 ± 0.1

249 nM for BIM$_{BH3}$, BIM$_{EL}$, and BAD, respectively (Figure 4B-E). We further confirmed the

250 specificity of these ABT-199 effects because the inhibition completely vanished when we

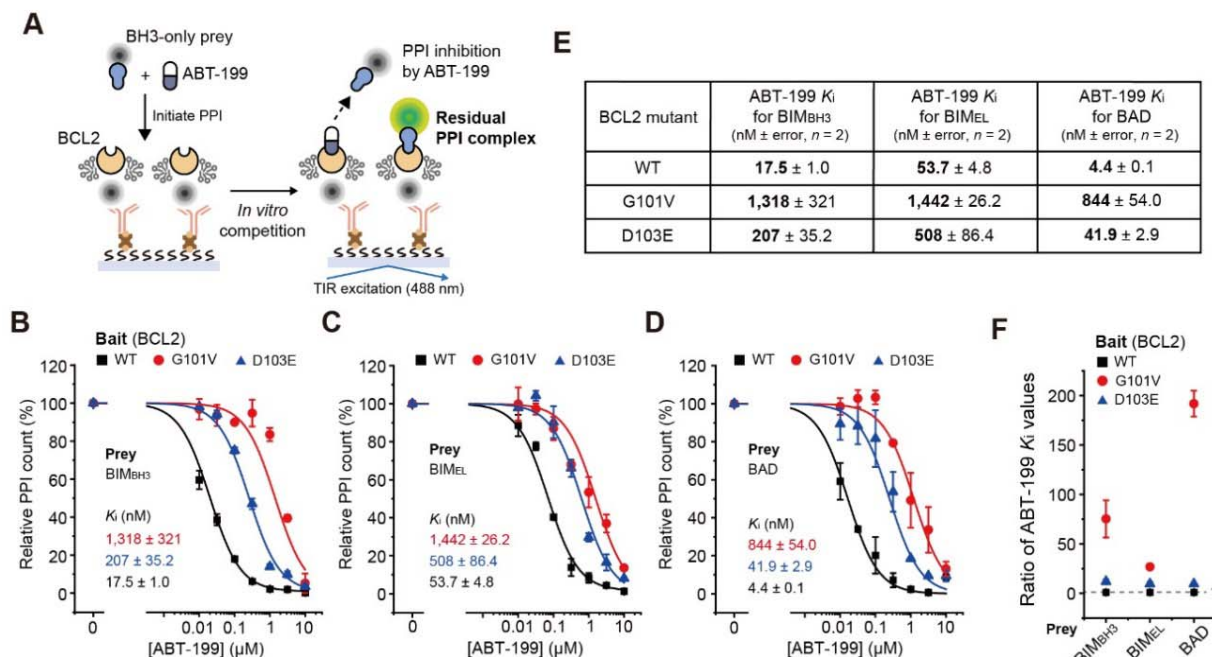251 switched the surface-immobilized bait to either BCLxL or MCL1 (Figure S7).

Figure 4. BCL2$_{G101V}$ and BCL2$_{D103E}$ take different routes to acquire resistance to ABT-199. (**A**) Schematic for the *in vitro* competition of ABT-199 with the PPIs between BCL2 and the BH3-only proteins. (**B-D**) Competitive ABT-199 inhibition curves for the residual PPI between each BH3-only protein to mutant BCL2s for K_i fitting. (B) BCL2-BIM$_{BH3}$ PPIs, (C) BCL2-BIM$_{EL}$ PPIs, and (D) BCL2-BAD PPIs. All data were fitted with equation (2) in the Methods section. (**E**) Fitted K_i for ABT-199 with each PPI pair. Each PPI signal is normalized to the corresponding ABT-199-untreated (0 μM) samples. Data are presented as means ± s.d. (n = 2). (**F**) Comparing the ratio of ABT-199 K_i values relative to BCL2$_{wt}$ PPIs.

Together, our SMPC data provide a compelling account for why CLLs with this *BCL2* mutation acquired resistance to ABT-199 treatment. In the presence of the BCL2 mutations tested, we observed a consistent shift in the inhibitory curves towards higher ABT-199 concentrations, indicating a reduced affinity of the BCL2 mutants for ABT-199 (Figure 4B-E). Notably, the G101V mutation, which diminished the interactions of BCL2 with BH3-only protein partners, similarly attenuated the binding to ABT-199. This attenuation was quantified as elevations in the K_i values by multiples of 75, 25, and 190 for BIM$_{BH3}$, BIM$_{EL}$, and BAD, respectively (Figure 4F). Remarkably, these K_i value increments for the G101V mutation far exceeded those of the K_d values for the corresponding PPIs (compare Figure 3F with Figure 4F), suggesting that the mutation's primary consequence is a diminished affinity for ABT-199 rather than an impaired ability to sequester BH3-only proteins. The D103E mutation exhibited a subtler decrease in ABT-199 affinity, with K_i values rising approximately tenfold for each of the three BH3-only proteins assessed (Figure 4B-F). While the D103E mutation maintained relatively high affinity for various pro-apoptotic proteins, it still showed significant increases in K_i values. An *in*

274 *silico* exploration of the D103E variant was carried out to elucidate the structural basis for its
275 differential impact on affinity for BIM_{BH3} and ABT-199 (Figure S8). Collectively, our SMPC
276 data elucidate the mechanisms by which CLL cells harboring the BCL2 mutation develop
277 resistance to ABT-199 therapy.

278

279 **Conclusion**

280 Our investigation utilized the SMPC platform to elucidate the interactions between BCL2 and its
281 mutants with an array of pro-apoptotic BH3-only proteins. The direct use of crude cell extracts is
282 a distinguishing advantage of this platform, significantly simplifying the experimental setup in
283 contrast to other methods for quantifying protein-protein interactions (PPIs). Our findings
284 indicate that when target proteins are overexpressed, endogenous proteins minimally interfere
285 with the target PPIs. This facilitates the omission of protein purification steps, which can be
286 laborious for mammalian proteins, while maintaining post-translational modifications and
287 avoiding the aggregation issues often encountered with membrane proteins and intrinsically
288 disordered regions.

289 The integration of eGFP and mCherry into our methodology has strengthened its
290 robustness and adaptability across diverse PPI studies. These fluorescent tags serve dual
291 functions as reporters and IP handles. Due to the ultra-high affinity of some commercial
292 antibodies for these tags, we achieved efficient IP within 15 minutes. Additionally, the absence
293 of homologs for these fluorescent proteins in mammalian proteomes virtually eliminated
294 nonspecific IP. A hurdle we encountered was the occasional proteolytic cleavage of the
295 fluorescent tags from their conjugated proteins. Nevertheless, since the cleaved fraction typically
296 represented less than 40% of the overall protein, we managed to adjust our calculated K_d and K_i
297 values with less than a two-fold correction. Future efforts will focus on optimizing the linker
298 sequence of these fluorescent tags to minimize such cleavage.

299 The imaging chips of our SMPC platform are designed for compatibility with standard
300 96- or 384-well plates, thus enabling parallel analysis of numerous PPIs. The reactions occur
301 near equilibrium within individual reaction chambers, and the use of a single-molecule TIR
302 fluorescence microscope equipped with auto-focusing enables PPI quantification by averaging

13

303   the single-molecule eGFP signals over 300 ms. We typically compile over more than ten images

304   per chamber to solidify our statistical confidence, rendering occupancy value determination for

305   each condition completed within a minute—a significant time reduction compared to western

306   blotting or surface plasmon resonance (SPR) analyses. Through this approach, we can derive K_d

307   and K_i values for complex multi-component interactions.

308   The scope of our study encompassed 21 PPI pairs involving BCL2 and its mutants. This

309   allowed for an in-depth analysis of the influence of the variably spliced N-terminal regions,

310   which are primarily disordered, on the affinity of BIM for BCL2. Furthermore, we characterized

311   the impact of BCL2 mutations found in relapsed CLL patients on the protein's interaction with

312   BH3-only proteins and the therapeutic agent ABT-199. Our research revealed that the mutations

313   G101V and D103E affect BCL2's interactions in notably distinct manners. While G101V impairs

314   the sequestration of pro-apoptotic proteins by BCL2, it significantly disrupts BCL2's affinity for

315   ABT-199, elucidating the pronounced resistance to the drug observed in CLL cases harboring

316   this mutation. Contrastingly, the D103E mutation either sustains or enhances the binding to

317   BH3-only proteins when compared to the wild type but exhibits a marked decrease in ABT-199

318   binding. We anticipate that the SMPC platform will be instrumental in the future analysis of

319   additional BCL2 mutations, particularly those in the second helix. In summary, the SMPC

320   platform's lower experimental demands, rapidity of measurement, and the quality and precision

321   of its data output poise it to be a pivotal tool in the generation of extensive, quantitative PPI

322   datasets.

Acknowledgement

Author Contribution

T.-Y.Y. conceived the project. C.C. and T.-Y.Y. designed the experiments. C.C. performed all experiments and analyzed data. C.C. performed data visualization. C.C. and T.-Y.Y. wrote the manuscript.

Competing Interests

The authors declare no competing financial interest.

Reference

1. Pawson, T.; Nash, P., Protein-protein interactions define specificity in signal transduction. *Genes Dev* **2000,** *14* (9), 1027-47.

2. Rolland, T.; Tasan, M.; Charloteaux, B.; Pevzner, S. J.; Zhong, Q.; Sahni, N.; Yi, S.; Lemmens, I.; Fontanillo, C.; Mosca, R.; Kamburov, A.; Ghiassian, S. D.; Yang, X.; Ghamsari, L.; Balcha, D.; Begg, B. E.; Braun, P.; Brehme, M.; Broly, M. P.; Carvunis, A. R.; Convery-Zupan, D.; Corominas, R.; Coulombe-Huntington, J.; Dann, E.; Dreze, M.; Dricot, A.; Fan, C.; Franzosa, E.; Gebreab, F.; Gutierrez, B. J.; Hardy, M. F.; Jin, M.; Kang, S.; Kiros, R.; Lin, G. N.; Luck, K.; MacWilliams, A.; Menche, J.; Murray, R. R.; Palagi, A.; Poulin, M. M.; Rambout, X.; Rasla, J.; Reichert, P.; Romero, V.; Ruyssinck, E.; Sahalie, J. M.; Scholz, A.; Shah, A. A.; Sharma, A.; Shen, Y.; Spirohn, K.; Tam, S.; Tejeda, A. O.; Trigg, S. A.; Twizere, J. C.; Vega, K.; Walsh, J.; Cusick, M. E.; Xia, Y.; Barabasi, A. L.; Iakoucheva, L. M.; Aloy, P.; De Las Rivas, J.; Tavernier, J.; Calderwood, M. A.; Hill, D. E.; Hao, T.; Roth, F. P.; Vidal, M., A proteome-scale map of the human interactome network. *Cell* **2014,** *159* (5), 1212-1226.

3. Huttlin, E. L.; Bruckner, R. J.; Paulo, J. A.; Cannon, J. R.; Ting, L.; Baltier, K.; Colby, G.; Gebreab, F.; Gygi, M. P.; Parzen, H.; Szpyt, J.; Tam, S.; Zarraga, G.; Pontano-Vaites, L.; Swarup, S.; White, A. E.; Schweppe, D. K.; Rad, R.; Erickson, B. K.; Obar, R. A.; Guruharsha, K. G.; Li, K.; Artavanis-Tsakonas, S.; Gygi, S. P.; Harper, J. W., Architecture of the human interactome defines protein communities and disease networks. *Nature* **2017,** *545* (7655), 505-509.

4. Deribe, Y. L.; Pawson, T.; Dikic, I., Post-translational modifications in signal integration. *Nat Struct Mol Biol* **2010,** *17* (6), 666-72.

5. Shaw, A. S.; Filbert, E. L., Scaffold proteins and immune-cell signalling. *Nat Rev Immunol* **2009,** *9* (1), 47-56.

6. Wright, P. E.; Dyson, H. J., Intrinsically disordered proteins in cellular signalling and regulation. *Nat Rev Mol Cell Biol* **2015,** *16* (1), 18-29.

7. Douzi, B., Protein-Protein Interactions: Surface Plasmon Resonance. *Methods Mol Biol* **2017,** *1615*, 257-275.

8. Helmerhorst, E.; Chandler, D. J.; Nussio, M.; Mamotte, C. D., Real-time and Label-free Bio-sensing of Molecular Interactions by Surface Plasmon Resonance: A Laboratory Medicine Perspective. *Clin Biochem Rev* **2012,** *33* (4), 161-73.

9. Patching, S. G., Surface plasmon resonance spectroscopy for characterisation of

membrane protein-ligand interactions and its potential for drug discovery. *Biochim Biophys Acta* **2014,** *1838* (1 Pt A), 43-55.

10.   Fernald, K.; Kurokawa, M., Evading apoptosis in cancer. *Trends Cell Biol* **2013,** *23* (12), 620-33.

11.   Carneiro, B. A.; El-Deiry, W. S., Targeting apoptosis in cancer therapy. *Nat Rev Clin Oncol* **2020,** *17* (7), 395-417.

12.   Kale, J.; Osterlund, E. J.; Andrews, D. W., BCL-2 family proteins: changing partners in the dance towards death. *Cell Death & Differentiation* **2018,** *25* (1), 65-80.

13.   Wei, M. C.; Zong, W. X.; Cheng, E. H.; Lindsten, T.; Panoutsakopoulou, V.; Ross, A. J.; Roth, K. A.; MacGregor, G. R.; Thompson, C. B.; Korsmeyer, S. J., Proapoptotic BAX and BAK: a requisite gateway to mitochondrial dysfunction and death. *Science* **2001,** *292* (5517), 727-30.

14.   Ren, D.; Tu, H. C.; Kim, H.; Wang, G. X.; Bean, G. R.; Takeuchi, O.; Jeffers, J. R.; Zambetti, G. P.; Hsieh, J. J.; Cheng, E. H., BID, BIM, and PUMA are essential for activation of the BAX- and BAK-dependent cell death program. *Science* **2010,** *330* (6009), 1390-3.

15.   Czabotar, P. E.; Westphal, D.; Dewson, G.; Ma, S.; Hockings, C.; Fairlie, W. D.; Lee, E. F.; Yao, S.; Robin, A. Y.; Smith, B. J.; Huang, D. C.; Kluck, R. M.; Adams, J. M.; Colman, P. M., Bax crystal structures reveal how BH3 domains activate Bax and nucleate its oligomerization to induce apoptosis. *Cell* **2013,** *152* (3), 519-31.

16.   Sarosiek, K. A.; Chi, X.; Bachman, J. A.; Sims, J. J.; Montero, J.; Patel, L.; Flanagan, A.; Andrews, D. W.; Sorger, P.; Letai, A., BID preferentially activates BAK while BIM preferentially activates BAX, affecting chemotherapy response. *Mol Cell* **2013,** *51* (6), 751-65.

17.   Robin, A. Y.; Krishna Kumar, K.; Westphal, D.; Wardak, A. Z.; Thompson, G. V.; Dewson, G.; Colman, P. M.; Czabotar, P. E., Crystal structure of Bax bound to the BH3 peptide of Bim identifies important contacts for interaction. *Cell Death Dis* **2015,** *6*, e1809.

18.   Shamas-Din, A.; Kale, J.; Leber, B.; Andrews, D. W., Mechanisms of action of Bcl-2 family proteins. *Cold Spring Harb Perspect Biol* **2013,** *5* (4), a008714.

19.   Del Gaizo Moore, V.; Letai, A., BH3 profiling--measuring integrated function of the mitochondrial apoptotic pathway to predict cell fate decisions. *Cancer Lett* **2013,** *332* (2), 202-5.

20.   Kelly, P. N.; Strasser, A., The role of Bcl-2 and its pro-survival relatives in tumourigenesis and cancer therapy. *Cell Death Differ* **2011,** *18* (9), 1414-24.

21.   Wang, H.; Guo, M.; Wei, H.; Chen, Y., Targeting MCL-1 in cancer: current status and

perspectives. *J Hematol Oncol* **2021,** *14* (1), 67.

22.   Kapoor, I.; Bodo, J.; Hill, B. T.; Hsi, E. D.; Almasan, A., Targeting BCL-2 in B-cell malignancies and overcoming therapeutic resistance. *Cell Death Dis* **2020,** *11* (11), 941.

23.   Lee, E. F.; Harris, T. J.; Tran, S.; Evangelista, M.; Arulananda, S.; John, T.; Ramnac, C.; Hobbs, C.; Zhu, H.; Gunasingh, G.; Segal, D.; Behren, A.; Cebon, J.; Dobrovic, A.; Mariadason, J. M.; Strasser, A.; Rohrbeck, L.; Haass, N. K.; Herold, M. J.; Fairlie, W. D., BCL-XL and MCL-1 are the key BCL-2 family proteins in melanoma cell survival. *Cell Death Dis* **2019,** *10* (5), 342.

24.   Westphal, D.; Kluck, R. M.; Dewson, G., Building blocks of the apoptotic pore: how Bax and Bak are activated and oligomerize during apoptosis. *Cell Death Differ* **2014,** *21* (2), 196-205.

25.   Hockings, C.; Alsop, A. E.; Fennell, S. C.; Lee, E. F.; Fairlie, W. D.; Dewson, G.; Kluck, R. M., Mcl-1 and Bcl-xL sequestration of Bak confers differential resistance to BH3-only proteins. *Cell Death Differ* **2018,** *25* (4), 721-734.

26.   Ku, B.; Liang, C.; Jung, J. U.; Oh, B. H., Evidence that inhibition of BAX activation by BCL-2 involves its tight and preferential interaction with the BH3 domain of BAX. *Cell Res* **2011,** *21* (4), 627-41.

27.   Cory, S.; Roberts, A. W.; Colman, P. M.; Adams, J. M., Targeting BCL-2-like Proteins to Kill Cancer Cells. *Trends Cancer* **2016,** *2* (8), 443-460.

28.   Ashkenazi, A.; Fairbrother, W. J.; Leverson, J. D.; Souers, A. J., From basic apoptosis discoveries to advanced selective BCL-2 family inhibitors. *Nat Rev Drug Discov* **2017,** *16* (4), 273-284.

29.   Tse, C.; Shoemaker, A. R.; Adickes, J.; Anderson, M. G.; Chen, J.; Jin, S.; Johnson, E. F.; Marsh, K. C.; Mitten, M. J.; Nimmer, P.; Roberts, L.; Tahir, S. K.; Xiao, Y.; Yang, X.; Zhang, H.; Fesik, S.; Rosenberg, S. H.; Elmore, S. W., ABT-263: a potent and orally bioavailable Bcl-2 family inhibitor. *Cancer Res* **2008,** *68* (9), 3421-8.

30.   Souers, A. J.; Leverson, J. D.; Boghaert, E. R.; Ackler, S. L.; Catron, N. D.; Chen, J.; Dayton, B. D.; Ding, H.; Enschede, S. H.; Fairbrother, W. J.; Huang, D. C.; Hymowitz, S. G.; Jin, S.; Khaw, S. L.; Kovar, P. J.; Lam, L. T.; Lee, J.; Maecker, H. L.; Marsh, K. C.; Mason, K. D.; Mitten, M. J.; Nimmer, P. M.; Oleksijew, A.; Park, C. H.; Park, C. M.; Phillips, D. C.; Roberts, A. W.; Sampath, D.; Seymour, J. F.; Smith, M. L.; Sullivan, G. M.; Tahir, S. K.; Tse, C.; Wendt, M. D.; Xiao, Y.; Xue, J. C.; Zhang, H.; Humerickhouse, R. A.; Rosenberg, S. H.; Elmore, S. W., ABT-199, a potent and selective BCL-2 inhibitor, achieves antitumor activity while sparing

platelets. *Nat Med* **2013,** *19* (2), 202-8.

31.   Tron, A. E.; Belmonte, M. A.; Adam, A.; Aquila, B. M.; Boise, L. H.; Chiarparin, E.; Cidado, J.; Embrey, K. J.; Gangl, E.; Gibbons, F. D.; Gregory, G. P.; Hargreaves, D.; Hendricks, J. A.; Johannes, J. W.; Johnstone, R. W.; Kazmirski, S. L.; Kettle, J. G.; Lamb, M. L.; Matulis, S. M.; Nooka, A. K.; Packer, M. J.; Peng, B.; Rawlins, P. B.; Robbins, D. W.; Schuller, A. G.; Su, N.; Yang, W.; Ye, Q.; Zheng, X.; Secrist, J. P.; Clark, E. A.; Wilson, D. M.; Fawell, S. E.; Hird, A. W., Discovery of Mcl-1-specific inhibitor AZD5991 and preclinical activity in multiple myeloma and acute myeloid leukemia. *Nat Commun* **2018,** *9* (1), 5341.

32.   Roberts, A. W.; Davids, M. S.; Pagel, J. M.; Kahl, B. S.; Puvvada, S. D.; Gerecitano, J. F.; Kipps, T. J.; Anderson, M. A.; Brown, J. R.; Gressick, L.; Wong, S.; Dunbar, M.; Zhu, M.; Desai, M. B.; Cerri, E.; Heitner Enschede, S.; Humerickhouse, R. A.; Wierda, W. G.; Seymour, J. F., Targeting BCL2 with Venetoclax in Relapsed Chronic Lymphocytic Leukemia. *N Engl J Med* **2016,** *374* (4), 311-22.

33.   Anderson, M. A.; Tam, C.; Lew, T. E.; Juneja, S.; Juneja, M.; Westerman, D.; Wall, M.; Lade, S.; Gorelik, A.; Huang, D. C. S.; Seymour, J. F.; Roberts, A. W., Clinicopathological features and outcomes of progression of CLL on the BCL2 inhibitor venetoclax. *Blood* **2017,** *129* (25), 3362-3370.

34.   Blombery, P.; Anderson, M. A.; Gong, J. N.; Thijssen, R.; Birkinshaw, R. W.; Thompson, E. R.; Teh, C. E.; Nguyen, T.; Xu, Z.; Flensburg, C.; Lew, T. E.; Majewski, I. J.; Gray, D. H. D.; Westerman, D. A.; Tam, C. S.; Seymour, J. F.; Czabotar, P. E.; Huang, D. C. S.; Roberts, A. W., Acquisition of the Recurrent Gly101Val Mutation in BCL2 Confers Resistance to Venetoclax in Patients with Progressive Chronic Lymphocytic Leukemia. *Cancer Discov* **2019,** *9* (3), 342-353.

35.   Birkinshaw, R. W.; Gong, J. N.; Luo, C. S.; Lio, D.; White, C. A.; Anderson, M. A.; Blombery, P.; Lessene, G.; Majewski, I. J.; Thijssen, R.; Roberts, A. W.; Huang, D. C. S.; Colman, P. M.; Czabotar, P. E., Structures of BCL-2 in complex with venetoclax reveal the molecular basis of resistance mutations. *Nat Commun* **2019,** *10* (1), 2385.

36.   Tausch, E.; Close, W.; Dolnik, A.; Bloehdorn, J.; Chyla, B.; Bullinger, L.; Dohner, H.; Mertens, D.; Stilgenbauer, S., Venetoclax resistance and acquired BCL2 mutations in chronic lymphocytic leukemia. *Haematologica* **2019,** *104* (9), e434-e437.

37.   Blombery, P.; Thompson, E. R.; Nguyen, T.; Birkinshaw, R. W.; Gong, J. N.; Chen, X.; McBean, M.; Thijssen, R.; Conway, T.; Anderson, M. A.; Seymour, J. F.; Westerman, D. A.;

Czabotar, P. E.; Huang, D. C. S.; Roberts, A. W., Multiple BCL2 mutations cooccurring with Gly101Val emerge in chronic lymphocytic leukemia progression on venetoclax. *Blood* **2020,** *135* (10), 773-777.

38.   Lee, H. W.; Ryu, J. Y.; Yoo, J.; Choi, B.; Kim, K.; Yoon, T. Y., Real-time single-molecule coimmunoprecipitation of weak protein-protein interactions. *Nat Protoc* **2013,** *8* (10), 2045-60.

39.   Yoo, J.; Lee, T. S.; Choi, B.; Shon, M. J.; Yoon, T. Y., Observing Extremely Weak Protein-Protein Interactions with Conventional Single-Molecule Fluorescence Microscopy. *J Am Chem Soc* **2016,** *138* (43), 14238-14241.

40.   Lee, H. W.; Kyung, T.; Yoo, J.; Kim, T.; Chung, C.; Ryu, J. Y.; Lee, H.; Park, K.; Lee, S.; Jones, W. D.; Lim, D. S.; Hyeon, C.; Heo, W. D.; Yoon, T. Y., Real-time single-molecule co-immunoprecipitation analyses reveal cancer-specific Ras signalling dynamics. *Nat Commun* **2013,** *4*, 1505.

41.   Lee, H. W.; Choi, B.; Kang, H. N.; Kim, H.; Min, A.; Cha, M.; Ryu, J. Y.; Park, S.; Sohn, J.; Shin, K.; Yun, M. R.; Han, J. Y.; Shon, M. J.; Jeong, C.; Chung, J.; Lee, S. H.; Im, S. A.; Cho, B. C.; Yoon, T. Y., Profiling of protein-protein interactions via single-molecule techniques predicts the dependence of cancers on growth-factor receptors. *Nat Biomed Eng* **2018,** *2* (4), 239-253.

42.   Choi, B.; Cha, M.; Eun, G. S.; Lee, D. H.; Lee, S.; Ehsan, M.; Chae, P. S.; Heo, W. D.; Park, Y.; Yoon, T. Y., Single-molecule functional anatomy of endogenous HER2-HER3 heterodimers. *Elife* **2020,** *9*.

43.   Adams, J. M.; Cory, S., The BCL-2 arbiters of apoptosis and their growing role as cancer targets. *Cell Death Differ* **2018,** *25* (1), 27-36.

44.   Hubner, A.; Barrett, T.; Flavell, R. A.; Davis, R. J., Multisite phosphorylation regulates Bim stability and apoptotic activity. *Mol Cell* **2008,** *30* (4), 415-25.

45.   Clybouw, C.; Merino, D.; Nebl, T.; Masson, F.; Robati, M.; O'Reilly, L.; Hubner, A.; Davis, R. J.; Strasser, A.; Bouillet, P., Alternative splicing of Bim and Erk-mediated Bim(EL) phosphorylation are dispensable for hematopoietic homeostasis in vivo. *Cell Death Differ* **2012,** *19* (6), 1060-8.

46.   Rooswinkel, R. W.; van de Kooij, B.; de Vries, E.; Paauwe, M.; Braster, R.; Verheij, M.; Borst, J., Antiapoptotic potency of Bcl-2 proteins primarily relies on their stability, not binding selectivity. *Blood* **2014,** *123* (18), 2806-15.

47.   Kvansakul, M.; Hinds, M. G., The Bcl-2 family: structures, interactions and targets for drug discovery. *Apoptosis* **2015,** *20* (2), 136-50.

48.   Mirdita, M.; Schutze, K.; Moriwaki, Y.; Heo, L.; Ovchinnikov, S.; Steinegger, M., ColabFold: making protein folding accessible to all. *Nat Methods* **2022**.

49.   Ruff, K. M.; Pappu, R. V., AlphaFold and Implications for Intrinsically Disordered Proteins. *J Mol Biol* **2021,** *433* (20), 167208.